Lawrence Berkeley National Laboratory
Recent Work

Title
Exchange bias due to coupling between coexisting antiferromagnetic and spin-glass orders

Permalink

Journal

ISSN

Authors
Maniv, E
Murphy, RA
Haley, SC
et al.

Publication Date

DOI

Copyright Information

Peer reviewed

Exchange bias due to coupling between coexisting antiferromagnetic and spin-glass orders

Eran Maniv,[1,2] Ryan A. Murphy,[1,3] Shannon C. Haley,[1,2] Spencer Doyle,[1] Caolan John,[1] Ariel Maniv,[4,5] Sanath K. Ramakrishna,[5] Yun-Long Tang,[1,6,2] Peter Ercius,[7] Ramamoorthy Ramesh,[1,6,2] Arneil P. Reyes,[5] Jeffrey R. Long,[1,2,8] and James G. Analytis[1,2]

[1]*Department of Physics, University of California, Berkeley, CA 94720, USA*

[2]*Materials Sciences Division, Lawrence Berkeley National Laboratory, Berkeley, California, 94720, USA*

[3]*Department of Chemistry, University of California, Berkeley, California 94720, USA*

[4]*NRCN, P.O. Box 9001, Beer Sheva, 84190, Israel*

[5]*National High Magnetic Field Laboratory, Tallahassee, Florida 32310, USA*

[6]*Department of Materials Science and Engineering, University of California, Berkeley, California 94720, USA*

[7]*National Center for Electron Microscopy, Molecular Foundry, Lawrence Berkeley National Laboratory, Berkeley, California 94720, USA*

[8]*Department of Chemical and Biomolecular Engineering, University of California, Berkeley, California 94720, USA*

(Dated: October 12, 2020)

Abstract

Exchange bias is a property of widespread technological utility, but whose underlying mechanism remains elusive, in part because it is rooted in the interaction of coexisting order parameters in the presence of complex magnetic disorder. Here, we show that a giant exchange bias housed within a spin-glass phase arises in a disordered antiferromagnet. The magnitude and robustness of the exchange bias emerges from a convolution of two energetic landscapes —— the highly degenerate landscape of the spin-glass biased by the sublattice spin-configuration of the antiferromagnet. The former provides a source of uncompensated moment, while the latter provides a mechanism for its pinning, leading to the exchange bias. Tuning the relative strength of the spin-glass and antiferromagnet order parameters reveals a principle for tailoring the exchange bias, with potential applications to spintronic technologies.

Technologies that leverage correlated properties of quantum materials are one of the most active areas of research at the boundary of physics and engineering. One such property is exchange bias. It is a critical component to a variety of devices such as spin-valves, used extensively in high density magnetic storage,[1] and has potentially more exotic applications, such as voltage-mediated magnetic switching for logic devices.[2] Exchange bias manifests itself as a shift in the hysteresis loop of a magnetic system when cooled under an applied external field,[3] and is observed in a diverse array of systems. Despite decades of study of the prototypical exchange bias system, thin film ferromagnetic/antiferromagnetic (FM/AFM) heterostructures, a complete understanding of the mechanism behind exchange bias is lacking. Recent work has revealed that pinned uncompensated moments generated by defects at the FM/AFM interface play a dominant role in engendering exchange bias, as well as in determining its magnitude.[4–6] The microscopic nature of the pinned uncompensated moment interface, how it is pinned by the AFM order parameter, and the mechanism by which this coupling drives exchange bias remains an outstanding challenge. Importantly, this interface may host its own "hidden" glassy order parameter, driven by spin frustration from disorder at the FM/AFM interface itself. Indeed, spin-glasses (SGs) alone may display exchange bias, and this in concert with studies on FM/SG interfaces have led to hypotheses suggesting that glassy dynamics are intertwined with exchange bias.[7–11]

SGs are a phase of matter occurring in many strongly correlated systems, but differ from ordered ferro- or antiferromagnets in that their ground state is metastable, being one of many nearly degenerate states.[12, 13] Central to these systems is frustration, which emerges as a result of site disorder[14, 15] or local competition between exchange interactions.[16] The frustration protects the ergodicity of the system until the SG transition is reached, at which point a metastable state is settled upon. Understanding the dynamic processes by which the glass traverses through this energetic landscape remains a major theoretical question in the statistical mechanics of solids. Theoretical challenges notwithstanding, the frozen state of the SG depends on its history, in particular the applied field in which it was cooled. This is the origin of its exchange bias: the magnetism of the frozen state is biased by the correlations of the SG. Typically this is very small, of the order of $0.01T$.

In this work, we leverage the highly field-responsive nature of the SG order parameter as a source of pinned uncompensated moment, and embed this within an anisotropic antiferromagnet. By isolating these phases in the *absence* of a nearby ferromagnet, we are explicitly able to study the exchange coupling between the AFM order parameter (defined as the sta-

bility of the sublattice magnetization) and the SG order parameter (defined as the breaking of ergodicity of fluctuating, disordered spins.[17]) Using the system Fe_xNbS_2 as an example, we show that when the uncompensated moments form a SG, there appear giant lateral shifts in the hysteresis loops. We find that the AFM order parameter biases the response of the SG, but only when *both* become long-time correlated. The origin of the exchange bias therefore lies in the convolution of two energy landscapes: the highly-degenerate landscape of the SG, biased by the sublattice phase space of the AFM. Further, our intercalation series allows us to tune the relative stability of both SG and AFM order parameters by changing the composition x, outlining novel design principles towards the development of new giant exchange bias phases.

Fe_xNbS_2 consists of triangular lattices of iron embedded between $2H$-NbS_2 layers. Single crystals were synthesized using conventional vapor transport techniques while varying concentrations of iron (see supplement sections 1-6 for characterization of homogeneity and stoichiometry). This material manifests AFM hexagonal ordering[18–20] with the moment predominantly oriented along the c-axis. For intercalation values less than $x = \frac{1}{3}$, SG-like behavior has been observed in magnetization and heat capacity measurements.[21–23] Magnetization versus temperature measurements performed along the c-axis on Fe_xNbS_2 for under- ($x = 0.30$) and over- ($x = 0.35$) intercalated values are shown in Figure 1a,c. For $x \approx \frac{1}{3}$, corresponding to the fully packed $Fe_{1/3}NbS_2$ structure, we observe a sharp AFM transition with a Néel temperature of approximately 42 K (see supplement section 14) as has been previously reported.[20, 22, 24–26] Above or below $x = \frac{1}{3}$, field cooled (FC) and zero field cooled (ZFC) curves begin to separate, indicating the presence of a frozen moment. The magnetization is observed to relax with time on removal of the applied field for such compositions, characteristic of SG behavior (Figure 1b,d).[13] The temperature onset of long relaxation times arises from the formation of an uncompensated moment, observed when FC and ZFC curves separate significantly. This temperature is roughly where the SG freezes on the time scale of the measurement, and the ergodicity of the system is broken; the spin configuration of the uncompensated moment is long-time correlated. Further experiments corroborating the glass state are detailed in the supplement (sections 6 ,9 ,10 and 12).

The disorder opens up a hysteresis loop whose center strongly depends on the cooling field. In Figure 2a,c, we illustrate the low temperature hysteresis loop for samples cooled in 7 T, and then field cycled across ± 7 T ten times. This 'training' of the hysteresis loop is consistent with exchange bias, and shows that the loop center becomes pinned at large fields;

approximately 3 T for $x = 0.30$, and 0.7 T for $x = 0.35$.[13, 27] In Figure 2b,d, we show enlargement of zero field cooled hysteresis loops, but with two different protocols for the field sweeps. For sweeps starting negative, 0→-7→+7→-7, the loop center shifts to positive field; for sweeps starting positive, 0→+7→-7→+7, the loop center moves to negative field. This spontaneous bias points to a history-dependent coupling scheme between the AFM and SG phases which is significantly more sensitive than in typical exchange bias systems.

Figure 3a,c show the temperature dependent evolution of H_{EB} (defined as the average of the zero magnetization-intercepts) and H_C (defined as the half width of the hysteresis loop at the average of the zero field-intercepts) which presents a non-trivial dependence. While the onset of H_C occurs at around the SG freezing temperature as expected, the bias H_{EB} onsets at a significantly lower temperature. The reason for this can be gleaned from measurements of nuclear magnetic resonance (NMR) spectra shown in Figure 4. The iron exchange field is studied via its effect on the ^{93}Nb lattice (with nuclear spin I = 9/2, γ = 10.405 MHz/T). In the paramagnetic state at temperatures $T > T_N$, the spectra exhibit a broad peak with quadrupolar splitting originating from two Nb unit cell sites. Below T_N the system splits into a double-peak structure around the paramagnetic center. This is a signature of AFM order, with the two peaks originating from the two sublattices where the local hyperfine field (approximately 1 T) adds to, and subtracts from, the externally applied magnetic field.[28] The peak structure onset significantly below T_N, suggesting it is only at these temperatures that the AFM order parameter is well formed. These lower temperatures correspond to the onset of H_{EB} seen in Figure 3a, a direct validation of the hypothesis that the exchange bias arises from the coexistence of the AFM order parameter with the SG. It is also notable that the peaks of dilute and excess intercalations are asymmetric (Figure 4a,c), in contrast to the stoichiometric case (Figure 4b), suggesting that coupling between the SG and AFM exerts an internal exchange field on the ^{93}Nb lattice: SG pinned uncompensated moments align with one AFM sublattice. This provides direct evidence for the existence of exchange coupling between the SG and the AFM order parameters.

Although the low field hysteresis loop is opened by the presence of disorder, the coupling to the antiferromagnetic order parameter means that it cannot close independently of the AFM. This motivates us to study the exchange bias at magnetic fields high enough to drive a metamagnetic transition in the AFM.[20] It has been recently shown that the AFM of the stoichiometric compound undergoes a metamagnetic transition from stripe to an up-up-up-down phase at $H_{plat} \sim 17$ T, which is characterized by a plateau in the magnetization.[20]

This same transition is observed at all compositions, albeit greatly broadened by disorder due to the deviation from $x = \frac{1}{3}$. As shown in Figure 5, hysteresis loops close only at fields that go well beyond the metamagnetic transition for any composition - the hysteretic response of the SG is coupled to the magnetic response of the AFM. Importantly, saturating the magnetization at these high fields also ensures that the sample is in the metamagnetic major loop. In conjunction with the spontaneous bias observed at both low and high fields (an effect incompatible with minor loops), these data show that the exchange bias observed cannot be attributed to minor loop effects. Low-field cooled loops are less easy to disentangle from minor loop phenomena, but their robust bias after multiple training loops is also inconsistent with minor loops (extended discussion in supplement section 11).

In order to see the effects of the field-cooled history, we study H_{EB} and H_C when the system is cooled in a field H_{FS}, and then cycled across $\pm H_{FS}$. As shown in Figure 3d, H_C tends to increase with higher H_{FS} for all compositions, suggesting that the exchange anisotropy of the SG grows as the field in which it was cooled increases, as in typical glassy systems. H_{EB} however is more directly correlated with the response of the AFM order. The $x = 0.30$ sample's peak exchange bias exceeds $H_{EB} \approx$ 3 T at relatively low fields, followed by a monotonic decrease at fields beyond H_{plat}, until no memory of magnetization history remains and $H_{EB} \to 0$ (Figure 3b). The $x = 0.31$ sample follows a similar trend but subsequently plateaus at high fields, suggesting a marginally more robust exchange bias (Figure 3b). For $x = 0.35$, H_{EB} shows a kink at the metamagnetic transition, but interestingly it saturates at high fields to around $H_{EB} \approx$ 1T, substantially higher than the diluted systems (Figure 3b). For an exchange bias, this is orders of magnitude greater than observed in typical heterostructure or SG systems,[13] but actually much closer to many theoretically predicted values in the absence of disorder.[29] The large bias is housed within the uncompensated moments of the SG, pinned by the coexisting AFM.

Our data suggests that the bias can be understood by considering the interplay of energy landscapes between the SG and AFM, as well as their exchange coupling. In the Sherrington-Kirkpatrick model, each possible state in an ergodic landscape of possible spin configurations is roughly interchangeable when looked at through the lens of spatial spin fluctuations. Above the SG transition, the accessible states are energetically equivalent. Below the SG transition, this ergodicity is broken by the freezing of the random spin texture.[17] However, the other possible states are only weakly distinguished in energy, so that effects like exchange bias which rely on restricting the accessible phase space volume are generally small (of the

order of 0.01T). In contrast, in an easy-axis AFM only one of two degenerate states is possible for a local spin, corresponding to distinct spin orientations. Indeed, experiments on the present system with an in-plane field $H//ab$, reveal significantly smaller H_{EB}, on the order of a typical SG exchange bias (see supplement section 13), confirming that the phase space of in-plane configurations is unaffected by the coexisting AFM. However, our measurements of giant exchange bias in the interlayer direction suggest that the coexistence of an AFM biases the glassy landscape, strongly distinguishing the possible spin states in energy by leveraging the sublattice broken symmetry of the AFM. This is the origin of the bias; in changing the landscape of the SG, the uncompensated moment becomes pinned by the coexisting texture of the AFM.

Our intercalation series further allows us to uniquely describe the roles that glassy disorder and AFM anisotropy play in exchange bias systems. A comparison of the relaxation dynamics indicates that the glass phase is more polarizable, thermally persistent, and relaxes more slowly as iron concentration decreases from over- to under-intercalated samples (Figure1b,d and supplement Figure S13). This trend follows the trend of the maximum amplitude of the exchange bias field: below the metamagnetic transition, the glassier samples are more responsive to their field history, resulting in a correspondingly larger exchange bias amplitude (Figure 3d). Above the metamagnetic transition, the relative stability of the AFM order parameter determines the robustness of the bias. In Figure 5 we show data from samples field-cooled at H_{FC}, but swept beyond $\pm H_{plat}$. This way, the effect of the field-cooled history of the SG can be separated from the effects of sweeping across the metamagnetic transition. As can be seen, in every case H_{EB} saturates at a single value at any field that exceeds H_{plat}, approaching 0 T, 0.3 T and 1 T for $x = 0.30$, 0.31 and 0.35 respectively (note, the figure shows examples of both 30 T and 35 T field sweeps, both greater than H_{plat}). These values are the same asymptotic values approached at high-field in Figure 3b, suggesting that the exchange bias of the SG depends on the ground state of the AFM.

The resilient, larger exchange bias that results from over-intercalation can be understood by considering its local structure. In the under intercalated samples, vacancies are introduced in the AFM lattice, whereas in the over intercalated sample the glass component instead sits on interstitial positions throughout the fully packed AFM structure. As the AFM component of the over-intercalated sample is fully intact, the anisotropy of the AFM and its ability to strongly bias the SG is retained even at high fields, resulting in a significantly larger exchange bias of approximately 1 T in comparison to the exchange bias plateau observed in

the $x = 0.31$ system. NMR experiments support a more robust AFM in over-intercalated samples: the AFM order parameter appears at higher temperatures and with more intact fine structure than the under-intercalated sample. This is further evidenced by heat capacity profiles, as under-intercalated samples are featureless, while the over-intercalated sample displays a broad peak (further discussion in supplement section 6). The nature of the defects determines how easily they can be pinned, and therefore the maximum bias value to the SG, but the robustness of the AFM determines the degree of this pinning, and therefore whether the exchange bias can be maintained at high magnetic fields. This division of labor demonstrates a strategy unique to the literature, and broadly applicable in the design of new giant exchange bias phases.

Classic exchange bias is thought to be driven by a "hidden" disordered FM/AFM interface, where pinned uncompensated moments are localized and pinned by the AFM phase.[5] Here, we remove the spectator FM phase in a unique circumstance of intertwined SG/AFM phases. The present system does not rely on pinning at just a thin film interface, but throughout the entire volume of the sample, essentially creating a *macroscopic* model interface, which reveals critical insight about general exchange bias mechanisms: the cooperative action of SG and AFM order compromises the ergodic landscape of the SG, forcing the uncompensated moment to be pinned to one sublattice. Importantly, the coexistence of SG and AFM phases has been established in multiple systems [30–33], and their interplay may have a direct connection to systems where disordered AFMs have been extensively studied in the context of the random-field Ising model.[34] In this case it is well established that random fields associated with disorder interact with the AFM lattice, directly influencing the avalanche of domain flips in applied magnetic fields.[35, 36] Random field models of exchange bias in bilayer systems, which build upon these foundations, indeed afford results that hew closely to experimental exchange bias data.[7, 29, 37] In this light, the intimate coupling between an uncompensated SG and a highly anisotropic AFM within a single crystal unsurprisingly results in exchange bias orders of magnitude larger than in bilayer systems. In principle, this mechanism also pertains to bilayer systems, and suggests a material design strategy that incorporates anisotropy and magnetic disorder as a path to larger bias materials with broader technological application.

METHODS

Single crystals of Fe_xNbS_2 were synthesized using a chemical vapor transport technique. A polycrystalline precursor was prepared from iron, niobium, and sulfur in the ratio $x : 1 : 2$ (Fe:Nb:S). The resulting polycrystalline product was then placed in an evacuated quartz ampoule with iodine as a transport agent (2.2 mg/cm^3), and put in the hot end of a two zone MTI furnace with temperature set points of 800 and 950 for a period of 7 days. High quality hexagonal crystals with diameters of several millimeters were obtained. Low field magnetization measurements were performed using a Quantum Design MPMS-3 system with a maximum applied magnetic field of 7 T. High field magnetization measurements were performed at NHMFL using a Vibrating Sample Magnetometry system with a maximum applied magnetic field of 35 T. NMR measurements were performed using the spin-echo technique, in the Condensed Matter NMR lab at NHMFL, using a home-built NMR spectrometer with quadrature detection. Measurements were done using the Hahn pulse sequence. The NMR signal was calculated by summing up the area below the echo peak. The magnetic field was varied between 6 T and 10 T at various temperatures from 4.2 K to 100 K. The magnet was calibrated using a standard current-field calibration curve, which is routinely checked with a calibrated sample. Heat Capacity measurements were performed using a XENSOR AC-sensor in a Cryogen-free magnet system. Powder X-ray diffraction measurements were performed using a Rigaku Ultima-4 system with a Cu K-α radiation. Energy dispersive X-ray spectroscopy was performed with an Oxford Instruments X-MaxN 50 mm^2 system. To perform inductively coupled plasma optical emission spectroscopy, the samples were first digested in hot 65% nitric acid, which was subsequently treated with an excess of HF to ensure complete dissolution of niobium, and the solutions were subsequently diluted to appropriate concentrations. A Perkin Elmer Optima 7000 DV ICP-OES was used to perform inductively coupled plasma optical emission spectroscopy.

DATA AVAILABILITY

Source data are available for this paper. All other data that support the plots within this paper and other findings of this study are available from the corresponding author on reasonable request.

ACKNOWLEDGMENTS

AUTHOR CONTRIBUTION

E.M., S.D., C.J. and S.C.H. performed crystal synthesis and magnetization measurements. E.M. performed heat capacity, EDS and micro-Laue measurements. R.A.M assisted in initial measurements and interpretation of glassy behavior and exchange bias, and performed ICP analysis. A.M., S.K.R. and A.P.R. performed NMR measurements. Y.L.T. and P.E. performed transmission electron microscopy measurements and analysis. E.M., R.A.M and J.G.A. performed data analysis and wrote the manuscript with input from all coauthors.

COMPETING INTERESTS

The authors declare no competing financial interests.

CORRESPONDENCE

Correspondence and requests for materials should be addressed to E.M. or J.G.A. (email: eranmaniv@berkeley.edu, analytis@berkeley.edu).

[1] Kools, J. Exchange-biased spin-valves for magnetic storage. *IEEE transactions on magnetics* **32**, 3165–3184 (1996).

[2] He, X. *et al.* Robust isothermal electric control of exchange bias at room temperature. *Nature materials* **9**, 579–585 (2010).

[3] Meiklejohn, W. H. & Bean, C. P. New magnetic anisotropy. *Physical review* **102**, 1413 (1956).

[4] Ohldag, H. *et al.* Correlation between exchange bias and pinned interfacial spins. *Physical review letters* **91**, 017203 (2003).

[5] Schuller, I. K., Morales, R., Batlle, X., Nowak, U. & Güntherodt, G. Role of the antiferro-magnetic bulk spins in exchange bias. *Journal of Magnetism and Magnetic Materials* **416**, 2–9 (2016).

[6] Kiwi, M. Exchange bias theory. *Journal of Magnetism and Magnetic materials* **234**, 584–595 (2001).

[7] Miltényi, P. *et al.* Diluted antiferromagnets in exchange bias: Proof of the domain state model. *Physical Review Letters* **84**, 4224 (2000).

[8] Ali, M. *et al.* Exchange bias using a spin glass. *Nature Materials* **6**, 70–75 (2007).

[9] Giri, S., Patra, M. & Majumdar, S. Related content Exchange bias effect in alloys and compounds. *J. Phys.: Condens. Matter* **23**, 73201–73224 (2011).

[10] Barnsley, L. C., Gray, M. & Webb, C. J. Recent citations Asymmetric reversal in aged high concentration CuMn alloy. *J. Phys.: Condens. Matter* **25**, 86003–86014 (2013).

[11] Hudl, M., Mathieu, R. & Nordblad, P. Tunable exchange bias in dilute magnetic alloys – chiral spin glasses. *Scientific Reports* **6**, 19964 (2016).

[12] Fischer, K. H. & Hertz, J. A. *Spin glasses*, vol. 1 (Cambridge university press, 1993).

[13] Mydosh, J. A. *Spin glasses: an experimental introduction* (CRC Press, 2014).

[14] Nagata, S., Keesom, P. & Harrison, H. Low-dc-field susceptibility of CuMn spin glass. *Physical Review B* **19**, 1633 (1979).

[15] Binder, K. & Young, A. P. Spin glasses: Experimental facts, theoretical concepts, and open questions. *Reviews of Modern physics* **58**, 801 (1986).

[16] Dekker, C., Arts, A., De Wijn, H., Van Duyneveldt, A. & Mydosh, J. Activated dynamics in a two-dimensional Ising spin glass: $Rb_2Cu_{1-x}Co_xF_4$. *Physical Review B* **40**, 11243 (1989).

[17] Parisi, G. Order parameter for spin-glasses. *Physical Review Letters* **50**, 1946 (1983).

[18] Van Laar, B., Rietveld, H. & Ijdo, D. Magnetic and crystallographic structures of Me_xNbS_2 and Me_xTaS_2. *Journal of Solid State Chemistry* **3**, 154–160 (1971).

[19] Suzuki, T., Ikeda, S., Richardson, J.W., Yamaguchi, Y. Magnetic Structure of $Fe_{1/3}NbS_2$. In *Proceedings of the Fifth International Symposium on Advanced Nuclear Energy Research*, 343–346 (1993).

[20] Haley, S. C. *et al.* Half-magnetization plateau and the origin of threefold symmetry breaking in an electrically switchable triangular antiferromagnet. *Phys. Rev. Research* **2**, 043020 (2020).

[21] Doi, N. & Tazuke, Y. Spin Glass Phases in $2H-Fe_xNbS_2$. *Journal of the Physical Society of Japan* **60**, 3980–3981 (1991).

[22] Yamamura, Y. *et al.* Heat capacity and phase transition of Fe_xNbS_2 at low temperature. *Journal of alloys and compounds* **383**, 338–341 (2004).

[23] Tsuji, T., Yamamura, Y., Watanabe, H., Saito, K. & Sorai, M. Heat capacity of intercalated layered materials Fe_xNbS_2 at low temperature. *Journal of thermal analysis and calorimetry* **57**, 839–846 (1999).

[24] Parkin, S. & Friend, R. 3d transition-metal intercalates of the niobium and tantalum dichalcogenides. II. Transport properties. *Philosophical Magazine B* **41**, 95–112 (1980).

[25] Friend, R., Beal, A. & Yoffe, A. Electrical and magnetic properties of some first row transition metal intercalates of niobium disulphide. *The Philosophical Magazine: A Journal of Theoretical Experimental and Applied Physics* **35**, 1269–1287 (1977).

[26] Little, A. *et al.* Three-state nematicity in the triangular lattice antiferromagnet $Fe_{1/3}NbS_2$. *Nature Materials* 1–6 (2020).

[27] Nogués, J. & Schuller, I. K. Exchange bias. *Journal of Magnetism and Magnetic Materials* **192**, 203–232 (1999).

[28] Büttgen, N., Kuhns, P., Prokofiev, A., Reyes, A. & Svistov, L. High-field NMR of the quasi-one-dimensional antiferromagnet $LiCuVO_4$. *Physical Review B* **85**, 214421 (2012).

[29] Malozemoff, A. Random-field model of exchange anisotropy at rough ferromagnetic-antiferromagnetic interfaces. *Physical review B* **35**, 3679 (1987).

[30] Wong, P.-z. *et al.* Coexistence of spin-glass and antiferromagnetic orders in the ising system $Fe_0.55Mg_0.45Cl_2$. *Physical review letters* **55**, 2043 (1985).

[31] Chillal, S. *et al.* Microscopic coexistence of antiferromagnetic and spin-glass states. *Physical Review B* **87**, 220403 (2013).

[32] Kleemann, W., Shvartsman, V., Borisov, P. & Kania, A. Coexistence of antiferromagnetic and spin cluster glass order in the magnetoelectric relaxor multiferroic $PbFe_0.5Nb_0.5O_3$. *Physical review letters* **105**, 257202 (2010).

[33] Fu, Z. *et al.* Coexistence of magnetic order and spin-glass-like phase in the pyrochlore antiferromagnet na 3 co (co 3) 2 cl. *Physical Review B* **87**, 214406 (2013).

[34] Young, A. P. *Spin glasses and random fields*, vol. 12 (World Scientific, 1998).

[35] Fishman, S. & Aharony, A. Random field effects in disordered anisotropic antiferromagnets. *Journal of Physics C: Solid State Physics* **12**, L729 (1979).

[36] Cardy, J. L. Random-field effects in site-disordered ising antiferromagnets. *Physical Review B* **29**, 505 (1984).

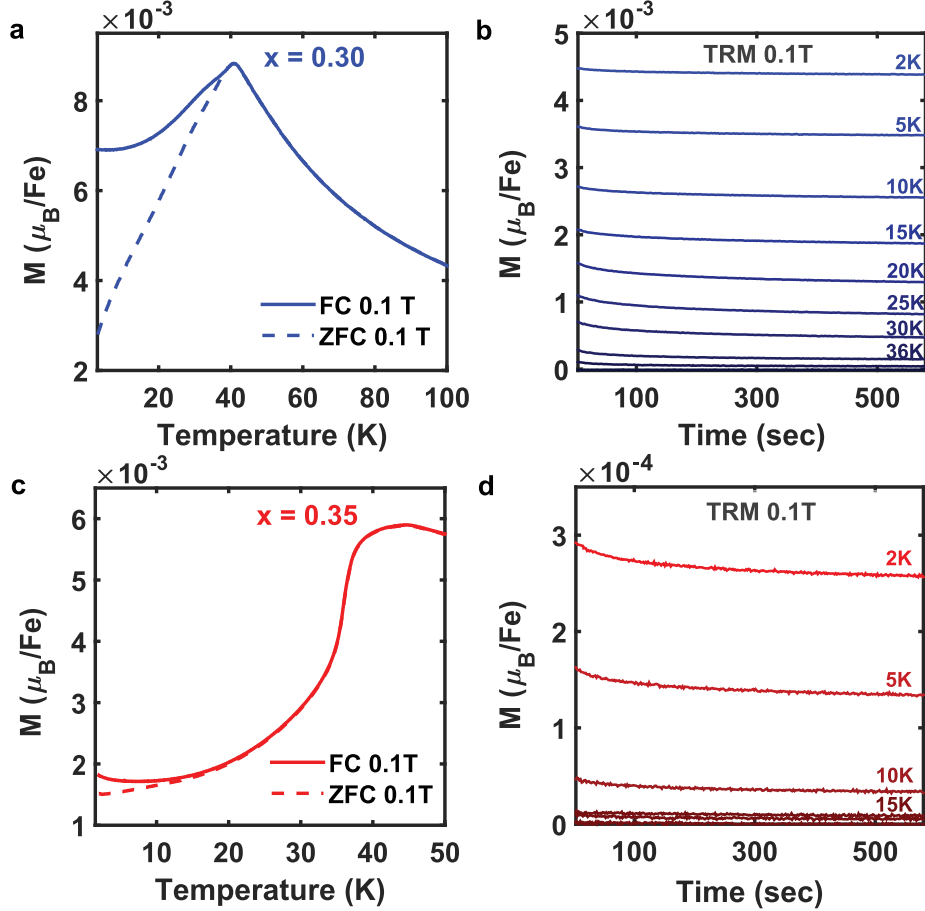[37] Malozemoff, A. Mechanisms of exchange anisotropy. *Journal of Applied Physics* **63**, 3874–3879 (1988).

FIG. 1. SG characterization of Fe_xNbS_2 for $x = 0.30$ and $x = 0.35$. (a),(c) 0.1 T magnetization versus temperature curves for each intercalation value: both the FC (solid line) and ZFC (dashed line) curves are shown. The AFM transition temperature (T_N) correlates to the sharp magnetization drop (approximately 41 K for x = 0.30 and 37 K for x = 0.35). The divergence of the FC and ZFC curves demonstrates the onset of a glassy frozen moment, which we identify as the effective SG freezing temperature (approximately 38 K for x = 0.30 and 15 K for x = 0.35). From Curie-Weiss fits we extract the effective moment to be 5.4, 5.2 and 5.4 μ_B/Fe for x = 0.30, 0.31 and 0.35 intercalations respectively (for full data and analysis see supplement section 8). (b),(d) Thermoremanent magnetization (TRM) measurements performed at various temperatures after field cooling the samples in a field of 0.1 T. The relaxation measurements are presented after the magnetic field was removed. The y-axis exhibits an order of magnitude difference between $x = 0.30$ (b) and $x = 0.35$ (d) intercalations. The appearance of relaxation dynamics is correlated with the glassy state. Additional isothermal remanent magnetization measurements, performed after zero field cooling the samples, present similar dynamics indicating a common relaxation mechanism in both routines (see supplement section 9 for full analysis).
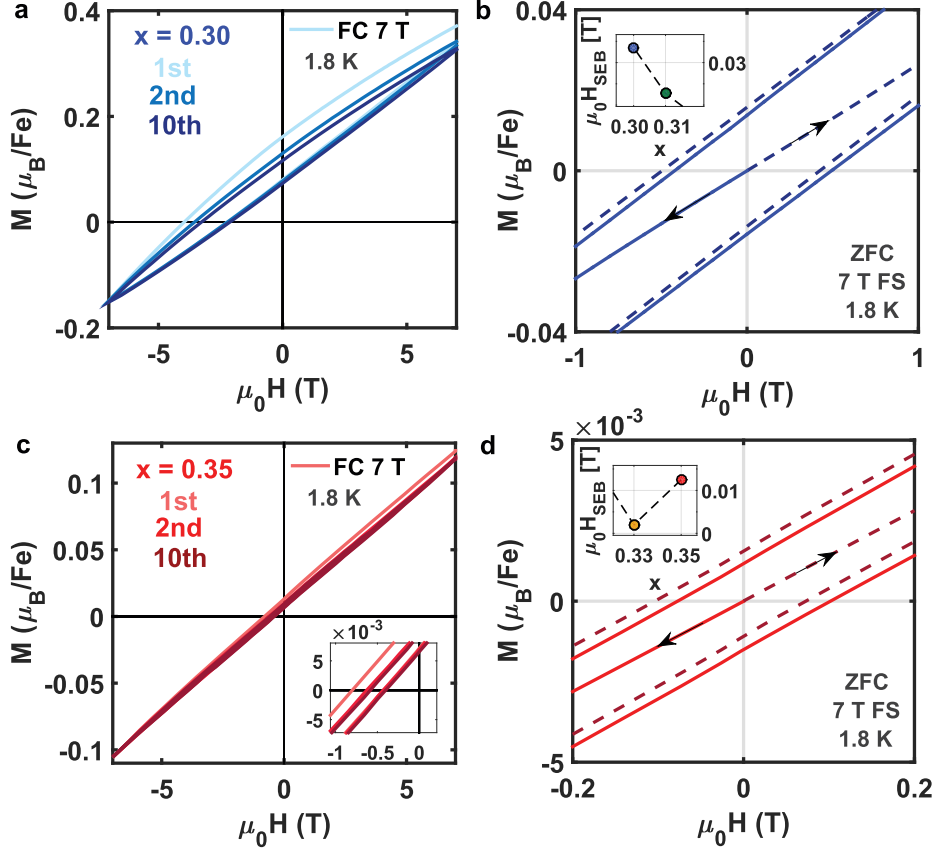
13

FIG. 2. Low field exchange bias characterization. (a),(c) Shifted magnetic hysteresis loops measured after cooling the samples from above the transition temperature. The slight decrease of the shifted hysteresis loops and their coercivity after 10 consecutive field sweeps demonstrates a training process in which the exchange bias is robust (see inset for $x = 0.35$ intercalation). (b),(d) Zoom-in on hysteresis loops taken at 1.8 K after cool-down without any external field. For each intercalation the magnetic field sweep was performed twice: starting the sweep in the negative direction (solid lines) or the positive one (dashed lines). A spontaneous exchange bias of a few 100 Oe which is dependent on the initial sweep direction is visible. Insets: The monotonic increase of the exchange bias field while departing the $x = \frac{1}{3}$ intercalation.
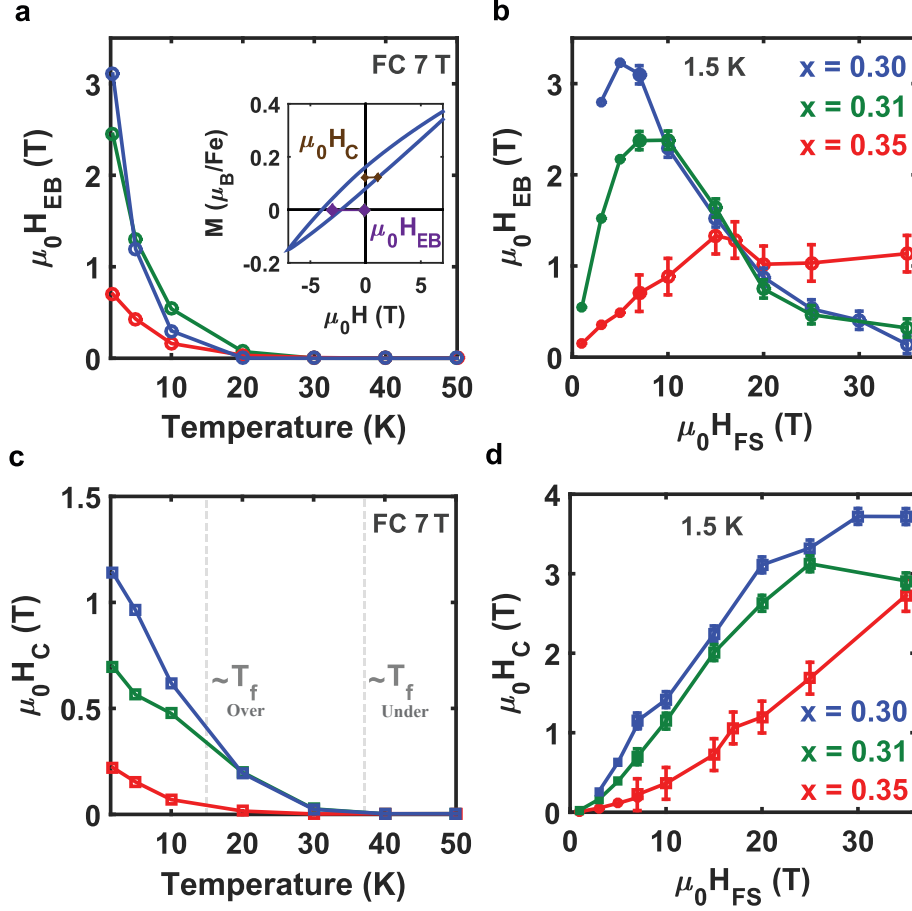
FIG. 3. The temperature and field sweep dependencies of the exchange bias. (a),(c) The temperature dependence of the extracted exchange bias and coercive fields for $x = 0.30, 0.31, 0.35$ intercalations, after cooling in a 7 T magnetic field from above the AFM transition. Inset (a): The exchange bias field (purple) was extracted from each loop by taking the average of the x-intercepts: $H_{EB} = \frac{H_{\text{int 1}} + H_{\text{int 2}}}{2}$. The coercive field (brown), H_C, was calculated from the half width of the hysteresis loop at the average of the y-intercepts. (c) The dashed lines mark the approximate SG freezing temperature for under(over)-intercalated samples, according to the FC/ZFC divergence presented in Figure 1a,c. (b),(d) The extracted exchange bias and coercive fields versus the sweeping field for $x = 0.30, 0.31, 0.35$ intercalations, measured at 1.5 K. The $x = 0.30$ intercalation was cooled in a 7 T magnetic field. For $x = 0.31, 0.35$ intercalations the cooling fields are identical to the field sweep range. H_{EB} shows a non-monotonic response as the swept field passes through the metamagnetic transition. For under-intercalated samples the exchange bias at high fields is suppressed, vanishing for $x = 0.30$ intercalation and saturating (around 0.3 T) for $x = 0.31$. Contrarily, for over-intercalation ($x = 0.35$) the high field exchange bias is saturated around 1 T. H_C grows monotonically with no distinct variation in the field range of the metamagnetic transition.
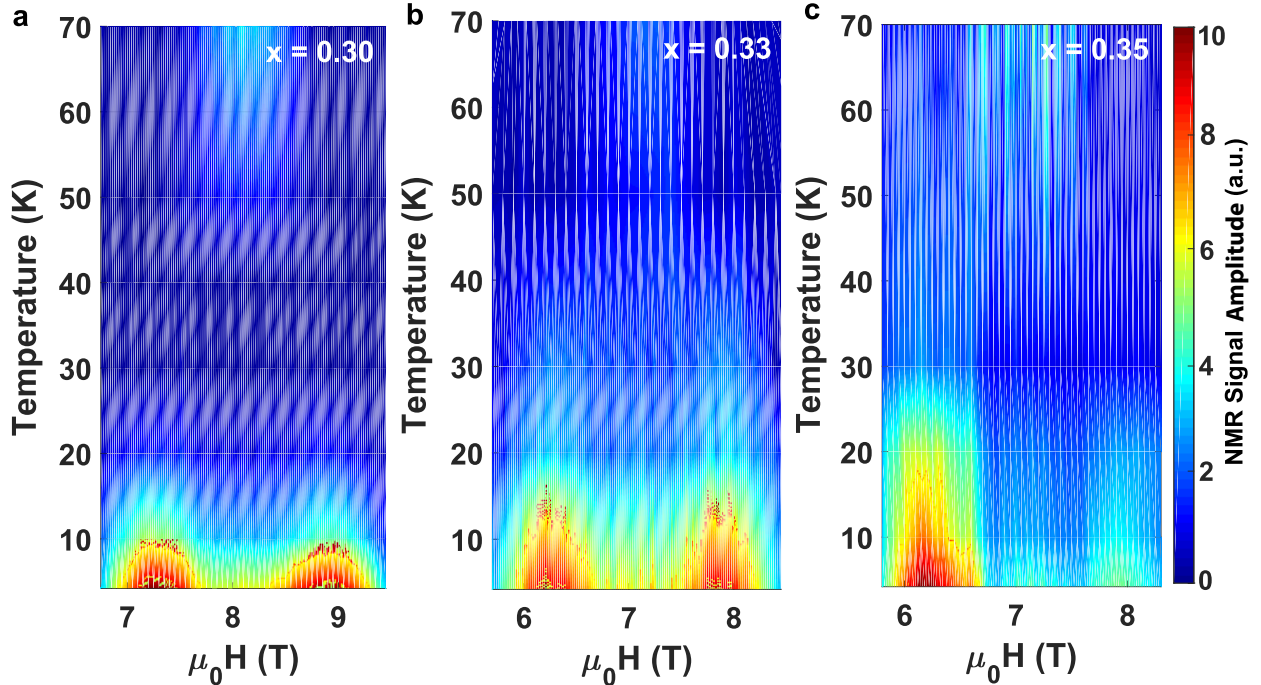
15

FIG. 4. NMR measurements performed on $x = 0.30, 0.33, 0.35$ intercalations. Field-swept NMR spectra at 85 MHz ($x = 0.30$) and 74.5 MHz ($x = 0.33, 0.35$) for several temperatures between 70 K to 4.2 K. The samples were cooled and measured in a magnetic field oriented along the c-axis. For $x = 0.30$ intercalation the 4.2 K field sweep was ZFC. The presented color maps of the NMR amplitude (normalized and scaled by their maximum value) are interpolations of the raw data. All samples show a single paramagnetic quadrupolar spectra at high temperatures which splits into two broad peaks at low temperatures due to AFM ordering. (a) As the temperature is lowered the Nb peaks broaden for the $x = 0.30$ sample. At temperatures below 20 K, two broad peaks indicative of a long-range AFM order emerge. Additionally, an asymmetry component between the two peaks is present. (b) The stoichiometric sample ($x = 0.33$) shows a similar peak structure but with no asymmetry. For this intercalation, the AFM phase is not affected by cooling in a magnetic field. (c) For the $x = 0.35$ sample the Nb peaks are clearly visible at all temperatures, indicating the iron lattice is highly ordered. Below 25 K, two broad peaks with a massive asymmetry component appear.
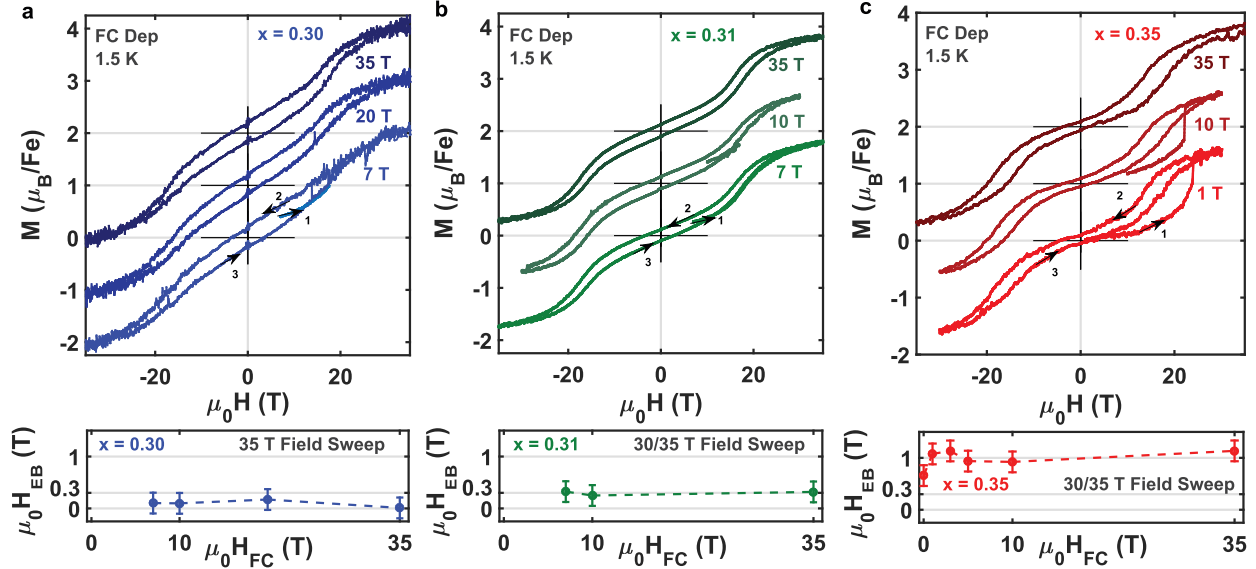
FIG. 5. High field exchange bias. Out-of-plane magnetization versus high magnetic field sweeps (up to 35 T) measured after cooling in various magnetic fields from above the AFM transition temperature down to 1.5 K. Each loop is offset on the y-axis by 1 μ_B/Fe. The arrows/numbers presents the sweep direction of the hysteresis loop for each intercalation. (a) The $x = 0.30$ sample does not show any significant exchange bias when swept up to 35 T in the range of the cooling fields taken (7 T - 35 T). (b) For the $x = 0.31$ sample, a stable exchange bias of approximately 0.3 T is captured in the same field range (7 T - 35 T). (c) Finally, the $x = 0.35$ sample shows a clear exchange bias of around 1 T at all implemented cooling fields (0 T - 35 T), demonstrating the high field sweep connection to the formation of exchange bias. Moreover, the metamagnetic transition clearly appears (on the initial field sweep direction) when the cooling field is weak enough, subsequently merging into the major hysteresis loop.